A Study on Skin Optics

Aravind Krishnaswamy and Gladimir V. G. Baranoski
Natural Phenomena Simulation Group, School of Computer Science, University of Waterloo, Canada

Technical Report CS-2004-01
January, 2004

Abstract

Despite the notable progress in physically-based rendering, there is still a long way to go before we can automatically generate predictable images of biological materials. In this report, we address an open problem in this area, namely the spectral simulation of light interaction with human skin. Initially, we present an overview of fundamental skin optics concepts which is followed by the description of a novel biophysically-based model that accounts for all components of light propagation in skin tissues, namely surface reflectance, subsurface reflectance and transmittance, and the biological mechanisms of light absorption by pigments in these tissues. The model is controlled by biologically meaningful parameters, and its formulation, based on standard Monte Carlo techniques, enables its straightforward incorporation into realistic image synthesis frameworks. Besides its biophysically-based nature, the key difference between the proposed model and the existing skin models is its comprehensiveness, *i.e.*, it computes both spectral (reflectance and transmittance) and scattering (bidirectional surface-scattering distribution function) quantities for skin specimens. In order to assess the predictability of our simulations, we evaluate their accuracy by comparing results from the model with actual skin measured data. We also present computer generated images to illustrate the flexibility of the proposed model with respect to variations in the biological input data, and its applicability not only in the predictive image synthesis of different skin tones, but also in the spectral simulation of medical conditions.

1 Introduction

The modeling of light interaction with human skin is relevant in a variety of fields such as medicine, cosmetic industry and realistic image synthesis. By studying processes involved in light remission from skin through computer simulations, better protocols can be developed to automatically diagnose medical conditions, such as jaundice (yellowish hue) [Rolinsky et al. 2001], erythema (redness) [Nischik and Forster 1997], as well as tumors at early stages [Cotton 1997]. Understanding how light is absorbed and propagated in skin tissues can assist in the design of lotions protective against harmful solar radiation, and also in the design of superior cosmetics. The games and entertainment industries can certainly benefit from being able to automatically generate realistic and predictable images of skin tissues. Creating believable images of human beings is usually an art entirely left to designers and animators. Artists currently model skin by carefully adjusting rendering parameters such as textures and colors. Despite its importance, the predictive rendering of organic materials, such as human skin, is still in its infancy, and many issues remain unsolved [Purgathofer 2003].

There is a considerable amount of research on skin optics available in the medical and biomedical literatures [Tuchin 2000], as well as recent investigations in pattern recognition [Nakai et al. 1998] and colorimetry [Doi and Tominaga 2003]. The modeling approaches used in these areas can be loosely classified into deterministic (*e.g.*, applying Kulbelka-Munk and diffusion theories [Anderson and Parrish 1981; Cotton 1997; Cotton and Claridge 1996; Diffey 1983; Doi and Tominaga 2003; van Gemert et al. 1989]) and nondeterministic (*e.g.*, applying Monte-Carlo methods [van Gemert et al. 1989; Churmakov et al. 2003; Flock et al. 1989; Meglinsky and Matcher 2001; Meglinsky and Matcher 2003; Nakai et al. 1998; Prahl 1988; Prahl et al. 1989; Shimada et al. 2001; Simpson et al. 1998; Tsumura et al. 2000; Wang et al. 1995; Wilson and Adam 1983; Yoon et al. 1987]). For a survey of these models, the interested reader is referred to the book by Tuchin [2000] and the thesis by Poirier [2004]. It is worth noting that these models are mostly aimed at the reproduction of skin spectral properties to determine the content and distribution of various substances [Tsumura et al. 2000; Zonios et al. 2001], *i.e.*, scattering properties affecting skin appearance are usually not addressed. Moreover, a substantial portion of the work done by the biomedical community is either laser-based or aimed at wavelengths outside the visible region of the light spectrum.

In computer graphics, the focus has been on developing scattering models to be incorporated into image synthesis frameworks. Although the application requirements are somewhat different, algorithms and techniques used in the models mentioned above have been incorporated in computer graphics. In 1993, Hanrahan and Krueger [1993] introduced to the graphics literature the algorithmic formulation for the simulation of tissue subsurface scattering proposed by biomedical researchers [Prahl 1988; Prahl et al. 1989; Wilson and Adam 1983], which consists on applying Monte Carlo methods to simulate light transport in organic tissue. Ng and Li [2001] extend the multilayer model proposed by Hanrahan and Krueger by adding a layer of oil on the outside of skin. Stam [2001] extended the work by Stamnes and Conklin [1984], which is based on discrete ordinate approximation of radiative transfers [Chandrasekhar 1960], in order to model a skin layer bounded by rough surfaces. Jensen *et al.* [2001] proposed a model for simulating multiple scattering subsurface light transport in translucent materials, including human skin, which uses a point source approximation based on the dipole method proposed by Farrel *et al.* [1992]. In addition, there has also been recent work in image based techniques for rendering and altering the appearance of skin [Tsumura et al. 2003].

Although the computer graphics skin models are biologically motivated, they do not simulate important biological processes, such as the absorption of light by natural chromophores (pigments), which are closely tied with skin spectral properties. As a result, they must rely on spectral parameters (*e.g.*, reflectance and transmittance) either set by the user or obtained in the literature, which are specimen specific and limited to a narrow range of illuminating and viewing geometries. It is important to note that there are also several other subsurface scattering models in the graphics literature which are either not biologically motivated or specifically designed to simulate other organic materials (*e.g.*, plants [Baranoski and Rokne 1997] and hair [Marschner et al. 2003]). An extensive review of these models is beyond the scope of this work, and the interested reader can find more information in a recent survey by Premoze [2002].

Clearly, the predictive simulation of both the spectral and the spatial distribution of the light incident on human skin is still an open problem not only in graphics, but also in biomedicine and colorimetry. In this report, we address this issue by proposing an algorithmic biophysically-based spectral model (henceforth referred to as BioSpec) specifically designed to account for the biological factors that affect light propagation and absorption in skin tissues. The BioSpec model is functionally comprehensive, *i.e.*, it takes as input biological and structural data and provides as output both spectral and scattering data for skin specimens. The former are provided in terms of reflectance

and transmittance values, while the later are given in terms of BSSDF (bidirectional surface-scattering distribution function), which can be decomposed into BRDF (bidirectional reflectance distribution function) and BTDF (bidirectional transmittance distribution function) components. The proposed model is controlled by biologically meaningful parameters determined through experiments described in the scientific literature, and its implementation, based on standard Monte Carlo Methods, enables its straightforward incorporation into most rendering frameworks. The spectral and scattering quantities can be either computed and used on the fly during the rendering process or stored in a database to be used off-line.

The remainder of this report is organized as follows. The next section describes the skin tissues and how they absorb and scatter light. Section 3 presents the algorithmic BioSpec model. Section 4 describes the approach used to evaluate the proposed model. Section 5 presents the results and discusses practical issues. Finally, Section 6 concludes the report and outlines directions for future work.

2 Light Interaction with Human Skin

Skin is a multilayered and inhomogeneous organ (Figure 1). In this section, we outline the biological characteristics of its main constituents, and how they affect the propagation and absorption of light.

2.1 Structural Characteristics and Spectral Properties

The first and outermost section of human skin is the stratum corneum, which is a stratified structure approximately 0.01-0.02 mm thick [Anderson and Parrish 1981; Meglinsky and Matcher 2001]. There are skin structural models, however, that consider it part of another tissue, namely the epidermis [Tuchin 2000] (Figure 1). The stratum corneum is composed mainly of dead cells, called corneocytes, embedded in a particular lipid matrix [Talreja et al. 2001]. Light absorption is low in this tissue, with the amount of transmitted light being relatively uniform in the visible region of the light spectrum [Everett et al. 1966].

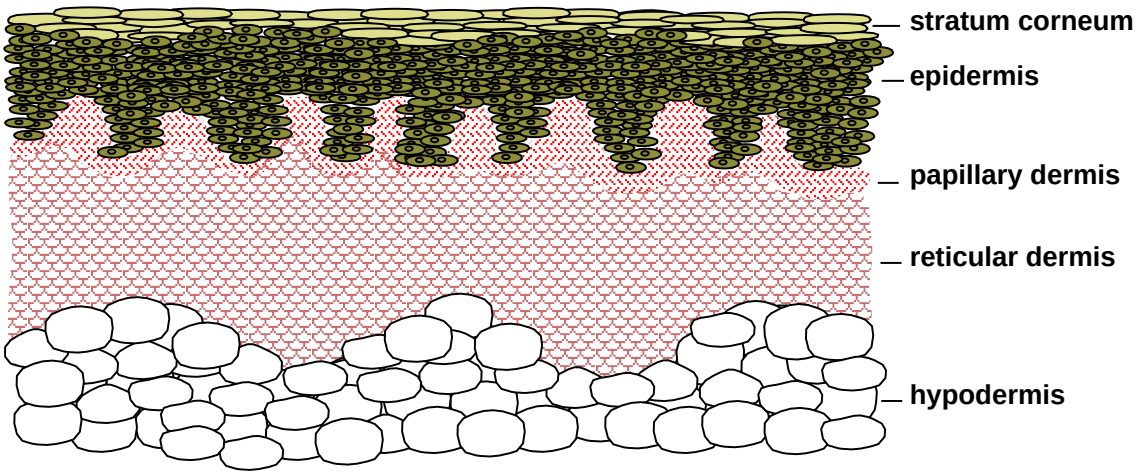

Figure 1: *Schematic cross-section of human skin tissues and the subcutaneous fat tissue (hypodermis).*

The epidermis is a 0.027-0.15mm thick structure [Anderson and Parrish 1981; Doi and Tominaga 2003; Meglinsky and Matcher 2001] composed of four layers (stratum basale, stratum spinosum, stratum granulosum and stratum lucidum). The epidermis propagates and absorbs light. The absorption property comes mostly from a natural chromophore, melanin. There are two types of melanin, the red/yellow phaeomelanin and a brown/back eumelanin [Thody et al. 1991]. Their absorption spectra are broad (Figure 2), with higher values for shorter wavelengths. The skin color is mostly associated with the eumelanin [Thody et al. 1991]. The ratio between the concentration of phaeomelanin and eumelanin present in human skin varies from individual to individual, with much overlap between skin types [Thody et al. 1991]. Recent studies reported values between 0.049 and 0.36 [Parsad et al. 2003]. Melanin is produced by cells called melanocytes occurring in the stratum basale, and it is found in membranous particles called melanosomes. The melanin absorption level depends on how many melanosomes per unit volume are in the epidermis. Typically, the volume fraction of the epidermis occupied by melanosomes varies from 1.3% (lightly pigmented specimens) to 43% (darkly pigmented specimens) [Jacques 1996].

The dermis is a 0.6-3mm thick structure [Anderson and Parrish 1981; Doi and Tominaga 2003; Meglinsky and Matcher 2001] which also propagates and absorbs light. It can be divided into two layers: the papillary dermis and the reticular dermis (Figure 1). These layers are primarily composed of dense, irregular connective tissue with nerves and blood vessels (smaller ones in the papillary, and larger ones in the reticular dermis). The volume fraction of blood in tissue can vary, roughly in the 0.2-7% range [Flewelling 1981; Jacques 1996]. The fluence rate of blood decreases as we get deeper into the skin, following an almost linear pattern in the dermis [van Gemert et al. 1989]. In the blood cells we find another natural chromophore, hemoglobin, which absorbs light and gives blood its reddish color. Normally, the hemoglobin concentration in whole blood is between 134 and 173g/L [Yaroslavsky et al. 2002]. In the arteries, 90-95% of hemoglobin is oxygenated, and in the veins, more than 47% of the hemoglobin is oxygenated [Angelopoulou 2001]. These two types of hemoglobin, namely oxygenated and deoxygenated hemoglobin, have slightly different absorption spectra (Figure 2). Two other blood borne pigments are found in the dermis, bilirubin and β-carotene, which contribute to the yellowish or olive tint of human skin (Figure 2). We remark that β-carotene may be also found in the epidermis and stratum corneum [Alaluf et al. 2002; Lee et al. 1975].

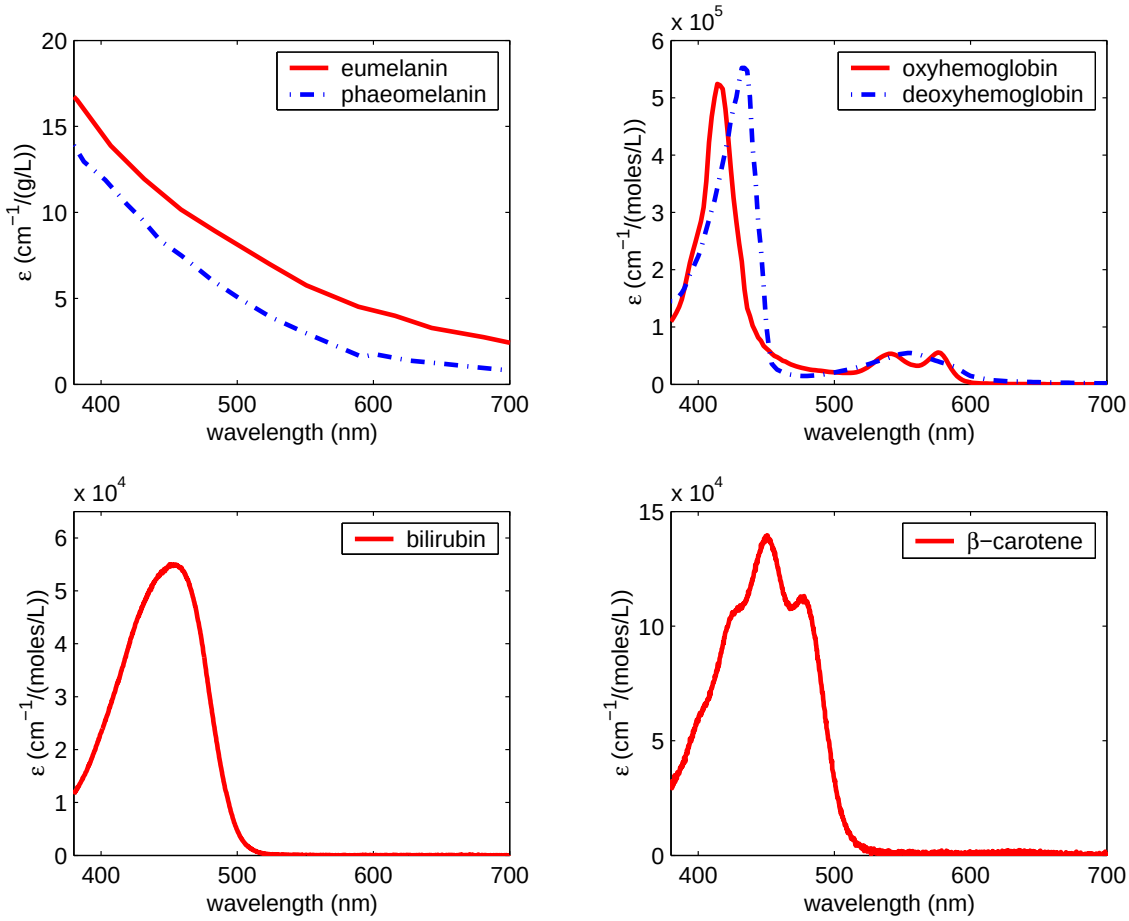

Figure 2: *Spectral extinction coefficient curves for the natural pigments present in skin tissues. Courtesy of S. Prahl and the Oregon Medical Laser Center (OMLC).*

The hypodermis is a subcutaneous adipose tissue characterized by a negligible absorption of light in the visible region of the spectrum [Flewelling 1981]. It is usually not considered part of the skin, and its size varies considerably throughout the body. It can be up to $3cm$ thick in the abdomen and absent in the eye lids. The hypodermis presents significant deposits of white fat, whose cells are grouped together forming clusters. Due to the presence of these white fat deposits, most of the visible light that reaches this tissue is reflected back to the upper layers [Doi and Tominaga 2003].

2.2 Scattering Profile

The scattering profile of human skin has two main components: surface and subsurface scattering. Surface scattering follows Fresnel equations [Su et al. 2002], and it is affected by the presence of folds in the stratum corneum. The aspect ratio of these mesostructures depends on biological factors such as aging and hydration [Talreja et al. 2001; Thalmann et al. 2002]. Approximately 5-7% of the light incident (over the entire spectrum) on the stratum corneum is reflected back to the environment [Tuchin 2000]. The remaining portion is transmitted to the internal tissues. Besides the reflective-refractive scattering caused by the reflection and refraction of light at cellular boundaries, two other types of subsurface scattering occur within the skin layers: Mie and Rayleigh scattering [Jacques 1996].

The stratum corneum and the epidermis are characterized as forward scattering media [Bruls and van der Leun 1984]. In the former this behavior is due to the alignment of the fibers, while in the later it is due to Mie scattering caused by particles that are approximately the same size of the wavelength of light (*e.g.*, cell organelles). The level of forward scattering for these tissues is wavelength dependent. Bruls and Leun [1984] performed goniometric experiments for five wavelengths for both the stratum corneum and the epidermis, and they showed that the scattering profiles are broader towards the shorter wavelengths.

In the dermis, collagen fibers (approximately $2.8\mu m$ in diameter and cylindrical [Jacques 1996]) are responsible for Mie scattering, while smaller scale collagen fibers and other micro-structures are responsible for Rayleigh scattering [Jacques 1996]. Light gets scattered multiple times inside the dermis before it is either propagated to another layer or absorbed. This means that the spatial distribution of the light scattered within the dermis quickly becomes diffuse [Anderson and Parrish 1981]. In fact, Jacques *et al.*, [1987] showed through goniophotometric measurements that backscattered light from the dermis is diffuse. While Mie scattering produces variations on both ends of the visible region of the light spectrum, Rayleigh scattering, being inversely proportional to the wavelength of light ($\approx \lambda^{-4}$), produces larger variations on the low end of the light spectrum [Jacques 1996; Glassner 1995].

3 The BioSpec Model

In the BioSpec model light propagation is described in terms of ray optics, and the wavelength of light, a physical optics [Glassner 1995] parameter essential for biophysically-based rendering applications, is included by associating a wavelength with each ray. The propagation of light in the skin tissues is simulated as a random walk process [Baranoski and Rokne 1997], whose states are associated with the following interfaces:

1. air ⇔ stratum corneum;
2. stratum corneum ⇔ epidermis;
3. epidermis ⇔ papillary dermis;
4. papillary dermis ⇔ reticular dermis;
5. reticular dermis ⇔ hypodermis.

Symbol	Definition
ξ_i	a uniform random number in the interval $[0, 1]$
p	ray free path length
r	radius of spheres used to represent collagen fibrils
η_s	index of refraction of stratum corneum
η_e	index of refraction of epidermis
η_p	index of refraction of papillary dermis
η_r	index of refraction of reticular dermis
η_f	index of refraction of collagen fibers in the dermis
η_m	index of refraction of the dermal medium
F	Fresnel coefficient
σ	aspect ratio of oblateness of stratum corneum folds
α	angle between normal of curved microarea and the normal of planar macrosurface
R_{sca}	Rayleigh scattering amount
t	thickness of a medium
θ	angle between ray direction and specimen's normal direction
a_1	stratum corneum total absorption coefficient
a_2	epidermis total absorption coefficient
a_3	dermis total absorption coefficient
a_{base}	baseline skin absorption coefficient
a_{cs}	stratum corneum absorption coefficient
a_{eu}	eumelanin absorption coefficient
a_{ph}	phaeomelanin absorption coefficient
a_{ce}	β-carotene absorption coefficient in epidermis
a_{ohb}	oxyhemoglobin absorption coefficient
a_{dhb}	deoxyhemoglobin absorption coefficient
a_{cd}	β-carotene absorption coefficient in dermis
a_{bil}	bilirubin absorption coefficient
c_{cs}	β-carotene concentration in stratum corneum
c_{eu}	β-carotene concentration in eumelanin
c_{ph}	β-carotene concentration in phaeomelanin
c_{hb}	concentration of hemoglobin in blood
c_{bil}	concentration of bilirubin in blood
ϑ_m	volume fraction of epidermis occupied by melanosomes
ϑ_p	volume fraction of papillary dermis occupied by whole blood
ϑ_r	volume fraction of reticular dermis occupied by whole blood
γ	ratio of oxyhemoglobin to the total hemoglobin concentration
t_s	thickness of the stratum corneum
t_e	thickness of the epidermis
t_p	thickness of the papillary dermis
t_r	thickness of the reticular dermis

Table 1: Symbols used in this report, in order of their appearance.

Once a ray hits the skin specimen at interface 1, it can be reflected back or refracted into the stratum corneum. ¿From there, the ray can be reflected and refracted multiple times within the skin layers before it is either absorbed or propagated back to the environment thru interface 1. Recall that the subcutaneous tissue is a highly reflective medium (Section 2.2). Hence, for body areas characterized by the presence of hypodermis, it is assumed total reflection at interface 5.

In the random walk implemented by the BioSpec model, the transition probabilities are associated with the Fresnel coefficients [Baranoski and Rokne 1997] computed at each interface (assuming that the cells are locally flat, *i.e.*, they are large with respect to the wavelength of

the incoming light), and the termination probabilities are associated with the free path length (p) computed when a ray travels in the skin layers. The model takes into account the three components of a skin specimen's BSSDF: surface reflectance, subsurface reflectance and transmittance. These components are affected by the refractive indices differences at the interfaces, tissue scattering and absorption of light by skin pigments. In the next sections we describe how each of these components is simulated. Due to the stochastic nature of the simulations, we use several random numbers which are uniformly distributed in the interval $[0, 1]$ and represented by ξ_i for $i = 1..11$.

3.1 Reflection/Transmission at the Interfaces

The Fresnel equations [Su et al. 2002] indicate how much light is reflected and transmitted at a plane surface as a function of the angle of incidence (θ_i) and the refractive indices of the incidence and transmissive media. Hence, the computation of the Fresnel coefficients requires the refractive indices of the stratum corneum, epidermis, papillary dermis and reticular dermis, which are denoted by η_s, η_e, η_p and η_r respectively.

After computing the Fresnel coefficient (F) at an interface, we obtain a random number ξ_1. If $\xi_1 \leq F$, then we generate a reflected ray, otherwise we generate a refracted ray. The reflected ray is computed applying the law of reflection, and the refracted ray is computed applying Snell's law [Baranoski and Rokne 1997; Glassner 1995].

3.2 Surface Scattering

A portion of the light that interacts with the stratum corneum cells is reflected back to the environment following the computation of the Fresnel coefficients described above. The spatial distribution of the reflected light varies according to the aspect ratio (or oblateness) of the stratum corneum folds (Section 2.2). We represent these mesostructures as ellipsoids whose aspect ratio ($\sigma \in [0, 1]$) is defined as the quotient of the length of the vertical axis by the length of the horizontal axis, which are parallel and perpendicular to the specimen's normal respectively. As the folds become flatter (lower σ), the reflected light becomes less diffuse. In order to account for this effect, we perturb the reflected rays using a warping function based on a surface-structure function proposed by Trowbridge and Reitz [1975], which represents rough air-material interfaces using microareas randomly curved. This surface-structure function is given by:

$$s_f = \frac{\sigma^4}{\sigma^2 \cos^2 \alpha + \sin^2 \alpha} \tag{1}$$

where:
σ = oblateness of the ellipsoid representing the curved microarea,
α = angle between the normal of the curved microarea and the normal of the planar macrosurface.

For $\cos \alpha$ varying from 0 to 1, s_f varies from σ^4 to 1. Hence, to obtain an angular warping function associated with the surface-structure function described above, we use the following approximation:

$$s_f = \sigma^4 - \sigma^4 \xi + \xi \tag{2}$$

where:
ξ = random number uniformly distributed in $[0, 1]$. from which we derive the polar perturbation angle given by:

$$\alpha = \arccos \left[\left(\frac{\sigma^2}{\sqrt{\sigma^4 - \sigma^4 \xi_2 + \xi_2}} - 1 \right)^{\frac{1}{2}} b \right]. \tag{3}$$

where:
b = $\frac{1}{\sigma^2 - 1}$.

3.3 Subsurface Scattering

When a ray enters either the stratum corneum or the epidermis, it is scattered (Section 2.2). Scattering in either of these layers involves the perturbation of the incoming ray in both the polar (α_f) and azimuthal (β_f) angles. The scattering with respect to the azimuthal angle β_f is expected to be symmetric (equal in all directions) [Prahl et al. 1989], thus we use $\beta_f = 2\xi_4\pi$. The scattering direction with respect to the polar angle α_f is computed using a randomized table look-up algorithm. Recall that Bruns and Leun [1984] have performed goniometric measurements for stratum corneum and epidermis (Section 2.2). The polar scattering angles measured at a given wavelength by Bruls and Leun [1984] are stored in a table, whose access indices correspond to the measured fractions of scattered radiation. For each ray we generate a random number ξ_5, which we multiply by the table size. The integer part of the resulting value is used to access the corresponding polar scattering angle stored in the table. This spectral data oriented approach provides higher accuracy results than the use of data-fitting functions [Baranoski et al. 2003]. [1]

It is possible for a ray to be warped such that it is reflected back to a previous layer. In this case there are few alternatives. First, we could just discard the ray, and consider it absorbed. Second, we could employ a rejection scheme to select only rays which are not reflected back to their previous layer. Third, we could continue to follow the ray, carefully accounting for the interface change again. Though the third alternative seems the most rigorous from an optics point of view, this phenomenon may not be justified from a biological standpoint. Recall that scattering is occuring as a ray travels through the medium, which means that if a ray is scattered to the previous layer, it will have happened at some point through the current layer. Since the ray will have travelled some portion within the medium, we must account for

[1] Bruls and Leun provide data for only two wavelengths. In the BioSpec model if $\lambda \leq 436nm$ we then use the 436nm scattering data, for $\lambda \geq 546nm$ we use the 546nm scattering data, and for $436nm < \lambda > 546nm$ we linearly interpolate the scattering data for 436nm and 546nm.

the probability that it may be absorbed. This adds an order of magnitude of complexity to the random walk process which can be avoided by selecting one of the other two alternatives. According to our experiments, employing a rejection scheme to select only rays that do not get scattered to previous layers provides a higher accuracy/cost ratio.

Every ray entering one of the dermal layers is initially tested for Rayleigh scattering (Section 2.2). The Rayleigh scattering simulation performed by the BioSpec model combines atmospheric optics [McCartney 1976] and skin optics [Jacques 1996] concepts. For a full derivation and discussion of the Rayleigh scattering equations used the reader is directed to the appendix.

In order to perform the Rayleigh test, we initially compute the spectral Rayleigh scattering amount (Equation 5), denoted by $R_{sca}(\lambda)$, which is associated with the probability that the Rayleigh scattering can occur [McCartney 1976]. We then generate a random number ξ_8. If $\xi_8 < 1 - \exp^{-R_{sca}(\lambda)}$, then the ray is scattered using polar (α_R) and azimuthal (β_R) perturbation angles. Since the Rayleigh phase function can be assumed to be symmetric in the azimuthal direction [McCartney 1976], the perturbation angles are given by:

$$(\alpha_R, \beta_R) = (\psi, 2\pi\xi_{10}) \tag{4}$$

where the angle ψ is obtained using rejection sampling in conjunction with the Rayleigh phase function [McCartney 1976]:

$$\begin{array}{ll} do & \\ & \psi = \pi\xi_9 \\ & \chi = \frac{3}{2}\xi_{10} \\ while & (\chi > \frac{3}{4}(1+\cos^2\psi)) \end{array}$$

According to Jacques [1996], collagen fibers occupy 21% of the dermal volume, and the Rayleigh scattering in this tissue can be approximated using spheres mimicing the ultrastructure associated with the random arrays of collagen fibrils of radius r. This results in a fiber density given by $N = 0.21(\frac{4}{3}r^3\pi)^{-1}$, which one can use to compute the spectral Rayleigh scattering amount through the following equation:

$$R_{sca}(\lambda) = \frac{8\pi^3((\frac{\eta_f}{\eta_m})^2 - 1)^2}{3N\lambda^4}\left(\frac{t}{\cos\theta}\right) \tag{5}$$

where:

η_f	=	index of refraction of the fibers,
η_m	=	index of refraction of the dermal medium,
t	=	thickness of the medium,
θ	=	angle ($< 90°$) between the ray direction and the specimen's normal direction.

Recall that light becomes diffuse in the dermis (Section 2.2). Hence, if the Rayleigh test fails or the ray has already been bounced off one of the dermal interfaces, then the ray is randomized around the normal direction using a warping function based on a cosine distribution [Baranoski and Rokne 1997]. [2] This warping function is given in terms of the polar (α_d) and azimuthal (β_d) perturbation angles as:

$$(\alpha_d, \beta_d) = (\arccos(\sqrt{\xi_6}), 2\pi\xi_7) \tag{6}$$

3.4 Absorption

When a ray travels in a given layer, it is first scattered as described in the previous section. The ray is then tested for absorption. If the ray is not absorbed, then it is propagated to the next layer. The absorption testing done by the BioSpec model is based on Beer's law [Tuchin 2000]. It is performed probabilistically every time a ray starts a run in a given layer. It consists of estimating the ray free path length (p) through the following expression:

$$p(\lambda) = -\frac{1}{a_i(\lambda)}\ln(\xi_{11})\cos\theta \tag{7}$$

where:

$a_i(\lambda)$	=	total absorption coefficient of pigments of given layer i,
θ	=	angle between the ray direction and the specimen's normal direction.

If $p(\lambda)$ is greater than the thickness of the pigmented medium (both expressed in cm), then the ray is propagated, otherwise it is absorbed. In the BioSpec formulation the thickness of the stratum corneum, epidermis, papillary dermis and reticular dermis are denoted by t_s, t_e, t_p and t_r respectively.

The BioSpec model accounts for the presence of eumelanin, phaeomelanin, oxyhemoglobin, deoxyhemoglobin, bilirubin and β-carotene. The spectral extinction coefficients for these pigments, denoted $\epsilon_{eu}(\lambda)$, $\epsilon_{ph}(\lambda)$, $\epsilon_{ohb}(\lambda)$, $\epsilon_{dhb}(\lambda)$, $\epsilon_{bil}(\lambda)$ and $\epsilon_{car}(\lambda)$ respectively, are obtained from the curves shown in Figure 2. The total absorption coefficient for each layer is simply the sum of the absorption coefficient for each pigment present in the layer, which is obtained by multiplying the pigment's spectral extinction coefficient by its estimated concentration in the layer.

It is difficult to accurately determine the baseline absorption coefficient for pigmentless skin tissues. Furthermore, due to its low magnitude [Saidi 1994] compared to the absorption coefficients of the skin chromophores, skin optics researchers usually assume that its effects are negligible [Angelopoulou 2001]. For the sake of completeness, however, we include the baseline skin absorption coefficient ($a_{base}(\lambda)$) in the absorption equations.

[2] Although intuitively the perturbation could be performed around the direction of propagation, according to our experiments, the perturbation around the normal direction introduces less bias in the randomization, and does not require any rejection scheme for rays that may be propagated towards the upper interface. Consequently, it also provides a higher accuracy/cost ratio.

The stratum corneum total absorption coefficient is given by:

$$a_1(\lambda) = a_{base}(\lambda) + a_{cs}(\lambda) \tag{8}$$

where:
$a_{cs}(\lambda)$ = β-carotene absorption coefficient.
The stratum corneum absorption coefficient a_{cs} is given by:

$$a_{cs}(\lambda) = \frac{\epsilon_{car}(\lambda)}{537} c_{cs} \tag{9}$$

where:
537 = molecular weight of beta-carotene ($g/mole$),
c_{cs} = β-carotene concentration in the stratum corneum ($\frac{g}{L}$).
The epidermis total absorption coefficient is given by:

$$a_2(\lambda) = (a_{eu}(\lambda) + a_{ph}(\lambda))\,\vartheta_m + (a_{base}(\lambda) + a_{ce}(\lambda))(1 - \vartheta_m) \tag{10}$$

where:
$a_{eu}(\lambda)$ = eumelanin absorption coefficient,
$a_{ph}(\lambda)$ = phaeomelanin absorption coefficient,
$a_{ce}(\lambda)$ = β-carotene absorption coefficient in the epidermis,
ϑ_m = volume fraction (%) of the epidermis occupied by melanosomes $\div 100$.
The absorption coefficient for eumelanin is given by:

$$a_{eu}(\lambda) = \epsilon_{eu}(\lambda) c_{eu} \tag{11}$$

where:
c_{eu} = eumelanin concentration ($\frac{g}{L}$).
Similarly, the absorption coefficient for phaeomelanin ($a_{ph}(\lambda)$) is computed by multiplying its spectral extinction coefficient ($\epsilon_{ph}(\lambda)$) by its concentration (c_{ph}). Also, the absorption coefficient a_{ce} is obtained by replacing c_{cs} by the concentration of β-carotene (c_{ce}) in the epidermis in Equation 9.
The papillary dermis total absorption coefficient is given by:

$$a_3 = (a_{ohb}(\lambda) + a_{dhb}(\lambda) + a_{cd}(\lambda) + a_{bil}(\lambda))\,\vartheta_p + a_{base}(\lambda)(1 - \vartheta_p) \tag{12}$$

where:
$a_{ohb}(\lambda)$ = oxyhemoglobin absorption coefficient,
$a_{dhb}(\lambda)$ = deoxyhemoglobin absorption coefficient,
$a_{cd}(\lambda)$ = β-carotene absorption coefficient in the dermal layers,
$a_{bil}(\lambda)$ = bilirubin absorption coefficient,
ϑ_p = volume fraction (%) of the papillary dermis occupied by whole blood $\div 100$.
The absorption coefficient a_{cd} is obtained by replacing c_{cs} by the concentration of β-carotene in the dermal layers (c_{cd}) in Equation 9. Also, recall that the volume fractions of blood vary within the dermis tissue (Section 2.1). Hence, to compute the reticular dermis total absorption coefficient (a_4), we replace ϑ_p by ϑ_r (volume fraction (%) of the reticular dermis occupied by whole blood $\div 100$) in Equation 12.
The absorption coefficient for oxyhemoglobin is given by:

$$a_{ohb}(\lambda) = \frac{\epsilon_{ohb}(\lambda)}{66500} c_{hb} * \gamma \tag{13}$$

where:
66500 = molecular weight of hemoglobin ($g/mole$),
c_{hb} = concentration of hemoglobin in the blood ($\frac{g}{L}$),
γ = ratio of oxyhemoglobin to the total hemoglobin concentration.
Similarly, the absorption coefficient for deoxyhemoglobin ($a_{dhb}(\lambda)$) is computed using its spectral extinction coefficient ($\epsilon_{dhb}(\lambda)$) and replacing γ by $(1 - \gamma)$ in Equation 13.
Finally, the absorption coefficient of bilirubin is given by:

$$a_{bil}(\lambda) = \frac{\epsilon_{bil}(\lambda)}{585} c_{bil} \tag{14}$$

where:
585 = molecular weight of bilirubin ($g/mole$),
c_{bil} = bilirubin concentration ($\frac{g}{L}$).

4 Evaluation Issues

Usually models of light interaction with matter are evaluated by visually inspecting the images generated using such models. Clearly, such an evaluation may be biased by factors not directly related to the model. For example, a careful modeling of skin's geometrical details [Haro

et al. 2001; Thalmann et al. 2002] and an accurate post-processing tone reproduction [Greenberg et al. 1997; Devlin et al. 2002] may improve the realistic appearance of skin specimens. These aspects, however, are addressed in other important areas of research, and they are beyond the scope of this work.

A current trend is to perform comparisons between model readings and measured data so that the models can be used in a predictive manner [Greenberg et al. 1997]. We used this approach in this work, *i.e.*, the BioSpec model was tested as a separated unit of the rendering pipeline and the results were compared with actual measured data [Everett et al. 1966; Marschner et al. 1999; Vrhel et al. 1994]. These comparisons were performed using a virtual spectrophotometer and a virtual goniophotometer [Baranoski and Rokne 1997], and reproducing the actual measurement conditions as faithfully as possible. The biophysical input data used in our experiments, unless otherwise stated in the text, is presented in Table 2.

The computer generated images presented in the next section serve two purposes. First, to illustrate the applicability of the BioSpec model in the spectral simulation of medical conditions associated with changes in the biophysical parameters. Second, to highlight an aspect for which measured data is scarce, namely the translucency of skin tissues. These images were rendered using a standard Monte Carlo path-tracing algorithm [Glassner 1995].

Parameter	Default Value	Source
r	$25nm$	[Li 2003]
η_s	1.55	[Anderson and Parrish 1981]
η_e	1.4	[Tuchin 2000]
η_p	1.36	[Jacques et al. 1987]
η_r	1.38	[Jacques et al. 1987]
η_f	1.5	[Jacques 1996]
t_s	$0.001cm$	[Anderson and Parrish 1981]
t_e	$0.01cm$	[Anderson and Parrish 1981]
t_p	$0.02cm$	[Anderson and Parrish 1981]
t_r	$0.18cm$	[Anderson and Parrish 1981]
c_{eu}	$80g/L$	[Thody et al. 1991]
c_{ph}	$12g/L$	[Thody et al. 1991]
c_{cs}	$2.1^{-4}g/L$	[Lee et al. 1975]
c_{ce}	$2.1^{-4}g/L$	[Lee et al. 1975]
c_{cd}	$7.0^{-5}g/L$	[Lee et al. 1975]
c_{hb}	$150g/L$	[Flewelling 1981]
c_{bil}	$0.05g/L$	[Rolinsky et al. 2001]
ϑ_m	5.2%	[Jacques 1996]
ϑ_p	1.2 %	[Angelopoulou 2001]
ϑ_r	0.91%	[Angelopoulou 2001]
γ	75 %	[Angelopoulou 2001]
σ	0.75	[Talreja et al. 2001; Thalmann et al. 2002]

Table 2: Data used in the evaluation of the BioSpec model.

5 Results and Discussion

Figure 3 presents comparisons of modeled reflectance curves provided by the BioSpec model with actual measured curves provided by Vrhel *et al.* [1994] (available in the North Carolina State University (NCSU) spectra database) for lightly and moderately pigmented specimens. The measurements were performed considering $\theta_i = 45°$ [Vrhel et al. 1994]. We can observe that the reflectance curves provided by the BioSpec model are qualitatively in agreement with the actual measured curves. The quantitative discrepancies may be due in part to the fact that the some parameters used in our simulations have to be estimated based on the overall description of the specimens (*e.g.*, in these experiments we set $\vartheta_m = 5.2\%$ and $\vartheta_m = 10\%$ for the lightly and moderately pigmented specimens respectively [Jacques 1996]). Furthermore, the exact position of the absorption peaks of the pigments depends on the solvents in which they are dissolved, and one can expect small shifts when comparing to *in vivo* values [Salisbury and Ross 1985].

The measured transmittance data for human skin available in the scientific literature, to the best of our knowledge, is limited to separated skin layers. Figure 4 presented comparisons between modeled and actual measured transmittance curves for the stratum corneum and epidermis tissues of two specimens, a moderately and a heavily pigmented one. The measured curves were provided by Everett *et al.* [1966], and they were obtained at a normal angle of incidence ($\theta_i = 0°$). Everett *et al.* [1966] reported thickness values for the moderately pigmented ($t_s = 0.0017cm$ and $t_e = 0.0025cm$) and the heavily pigmented ($t_s = 0.0023cm$ and $t_e = 0.0021cm$) specimens. Based on their description of the specimens, we set $\vartheta_m = 9.5\%$ and $\vartheta_m = 38\%$ for the lightly and heavily specimens respectively. Again, we can observe a qualitative agreement between the modeled and the actual measured curves. The quantitative discrepancies, also related to the factors mentioned above, are noticeable but within acceptable accuracy boundaries since the measured curves have a reported tolerance of $\approx \pm 5\%$ [Everett et al. 1966].

The overall reflectance of human skin presents interesting features. As expected, darker skin (characterized by higher volume fractions of epidermis occupied by melanosomes) reflects less light than lighter skin. However, lightly pigmented skin presents a characteristic "W" shape in the reflectance curves between $500nm$ and $600nm$ [Angelopoulou 2001]. Oxygenated hemoglobin is responsible for this feature, which can be accentuated as the proportion of oxyhemoglobin with respect to total hemoglobin increases [Zonios et al. 2001]. The graphs presented in Figure 5 indicate that the BioSpec model can capture these optical characteristics of human skin.

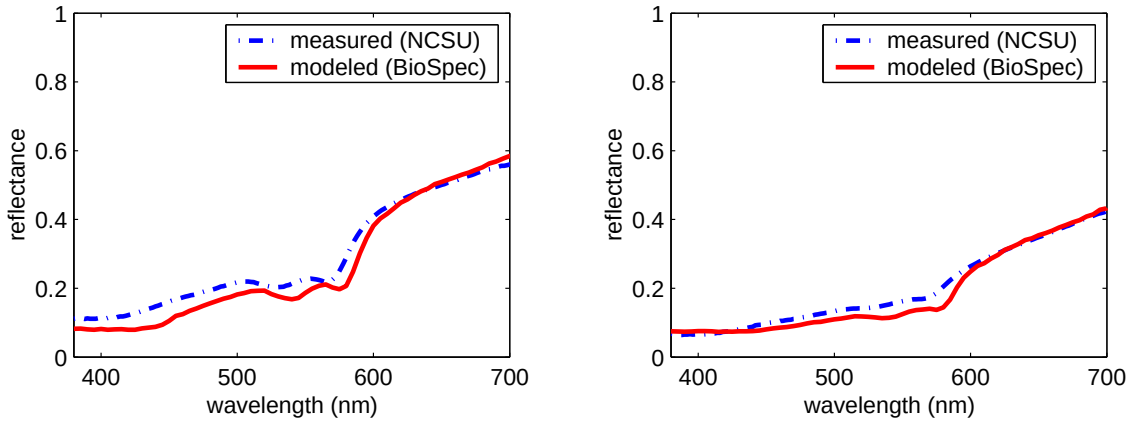

Figure 3: *Comparison of modeled reflectance curves provided by the BioSpec model with actual measured curves available in the NCSU spectra database by Vrhel [1994]. Left: lightly pigmented skin specimen (NCSU file 113). Right: moderately pigmented specimen (NCSU file 82).*

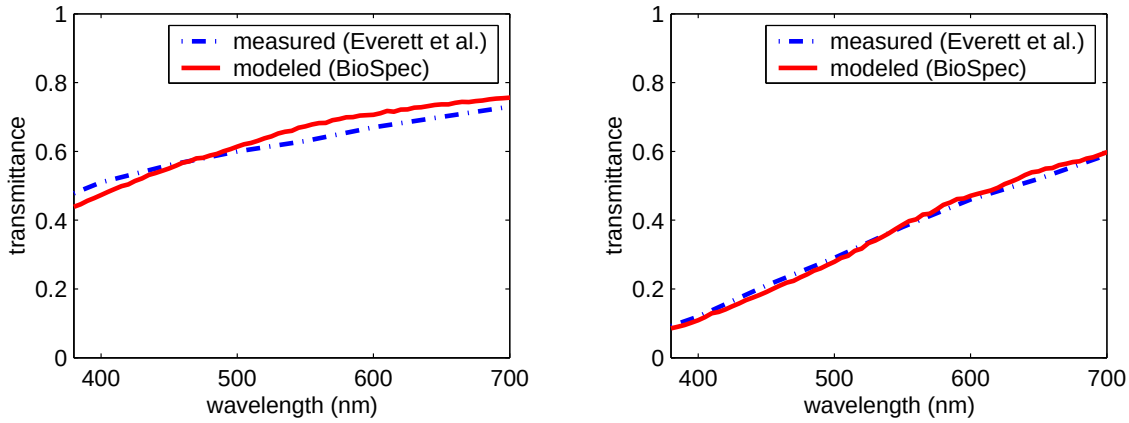

Figure 4: *Comparison of modeled transmittance curves (for the stratum corneum and epidermis tissues) provided by the BioSpec model with actual measured curves provided by Everett et al. [1966]. Left: moderately pigmented specimen. Right: heavily specimen.*

Figure 6 shows a comparison between modeled and actual measured skin BRDFs provided by Marschner *et al.* [1999]. Since the BioSpec model provides spectral readings, we needed to integrate spectral values over the visible region of the light spectrum in order to obtain data that could be compared to the data provided by Marschner *et al.* [1999]. Based on the lightly pigmented specimen's description provided by Marschner *et al.* [1999], we set $\vartheta_m = 2.5\%$ in these experiments. As illustrated by the measurements provided by Marschner *et al.* [1999] (Figure 6 (left)), the BRDF of skin specimens presents an angular dependence, and it becomes more diffuse for small angles. Figure 6 (right) shows that the BioSpec model can represent this angular dependency, and the modeled BRDF curves generally agree with the measured BRDF curves provided by Marschner *et al.* [1999]. The most noticeable quantitative discrepancies are observed for the larger angle of incidence, namely $\theta_i = 60°$. It is worth noting, however, that besides the previously mentioned factors that quantitatively affect the modeled curves, one should also consider the sources of noise in the measurements performed by Marschner *et al.* [1999], which include deviations in the specimen's normal estimation and spatial variations in the measured BRDFs.

Skin specimens characterized by thin and numerous folds (*e.g.*, young and/or hydrated specimens) present a directional behavior stronger than specimens with wider but fewer folds (*e.g.*, old and/or dry specimens) [Marschner et al. 1999; Talreja et al. 2001; Thalmann et al. 2002]. The former case corresponds to folds with lower aspect ratio, while the later case corresponds to folds with a higher aspect ratio [Talreja et al. 2001; Thalmann et al. 2002]. Figure 7 presents modeled BRDF curves for two angles of incidence, namely $\theta_i = 15°$ and $\theta_i = 45°$, obtained by varying the parameter σ associated with the folds' aspect ratio. These curves show that the BioSpec model can qualitatively simulate the variation in the scattering behavior of skin specimens associated with changes in the aspect ratio of the stratum corneum folds.

A mechanical, chemical, electrical, thermal or luminous stimulus can induce a reddening around the stimulation site on the skin. This abnormal redness of the skin, which may be also due to an inflammation [Tuchin 2000], is caused by a dilation of the blood vessels followed by an increase in the volume fractions of blood in the dermal layers. Figure 8 shows images generated to illustrate the capability of the BioSpec model of spectrally simulate this medical condition by varying, within actual biological limits, the parameters associated with the increase of the volume fractions of blood in the papillary (ϑ_p) and reticular (ϑ_r) dermis.

Jaundice, or hyperbilirubinemia [Rolinsky et al. 2001; Saidi 1994], is a medical symptom associated with the accumulation of bilirubin in the dermal tissues. It is usually caused by liver or gall bladder disorders, and it is characterized by the yellowish appearance of the skin and eyes. Figure 9 shows images generated to illustrate the capability of the BioSpec model of spectrally simulate this medical symptom by

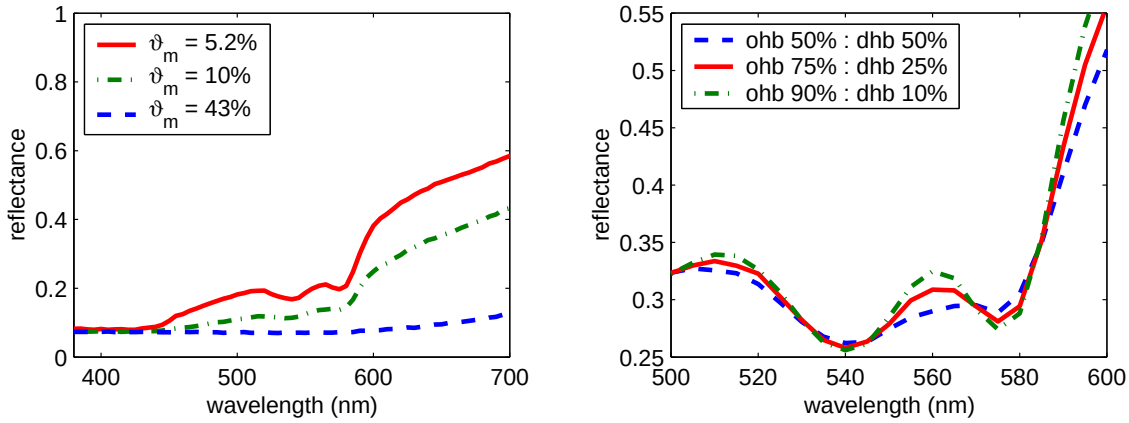

Figure 5: *Comparison of modeled spectral curves provided by the BioSpec model ($\theta_i = 45°$) considering the variation of biological parameters. Left: volume fractions of epidermis occupied by melanosomes (ϑ_m). Right: ratio of oxygenated (ohb) to deoxygenated (dhb) hemoglobin in the dermal layers.*

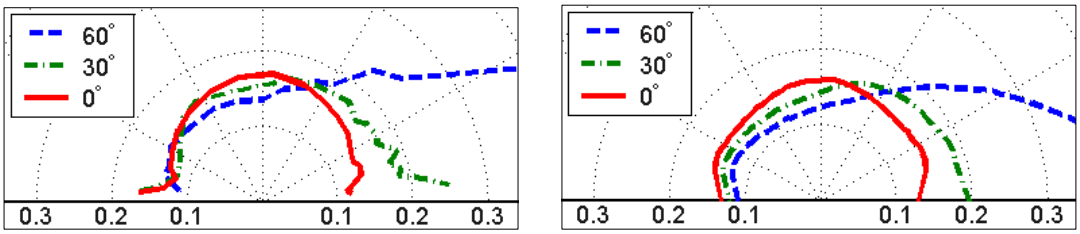

Figure 6: *Comparison of BRDF curves for a lightly pigmented specimen. Left: actual measured BRDF curves provided by Marschner et al. [1999]. Right: modeled BRDF curves provided by the BioSpec model.*

varying, within actual biological limits, the parameters associated with the increase of bilirubin concentration (c_{bil}) in the dermal layers.

The BTDF of the whole skin can be observed (*in vivo*) in body parts with a thin or absent hypodermis, such as ears, eye lids and fingers. In these areas the behavior of the transmitted light is near Lambertian, to the point where no internal structure can be noticeable [Rodriguez et al. 2002]. Figure 10 presents images generated using the BioSpec model to illustrate the translucency of skin tissues as well as its variations due to different melanin pigmentation levels.

6 Conclusion and Future Work

We presented an overview of fundamental skin optics concepts as well as a novel biophysically-based model for light interaction with human skin. It provides both spectral and scattering data for skin specimens, and it is controlled by biologically meaningful parameters. Results from the model were compared with results from actual experiments. These comparisons showed good agreement between modeled and measured data, and strengthened our confidence in the predictability of the proposed model. They also suggested that there is still room for improvement.

As future work, from a scattering point of view, we intend to investigate factors affecting the anisotropy of skin specimens, such as the presence of wrinkles. External factors, such as cosmetics, oil and sweat, may affect the skin's BRDF and light polarization. These factors will be examined in the next stage of our research as well. From a spectral point of view, we plan to extend the model's scope to the ultraviolet and infrared regions of the light spectrum and incorporate time dependent mechanisms of photon reemission. These features would allow us to use the proposed model in the visual simulation of biological processes affecting both the appearance and health of human skin such as fluorescence, tanning and the formation of melanomas.

References

ALALUF, S., HEINRICH, U., STAHL, W., TRONNIER, H., AND WISEMAN, S. 2002. Dietary carotenoids contribute to normal human skin color and uv photosensitivity. *Journal of Nutrition 132*, 399–403.

AMEEN, D. B., BISHOP, M. F., AND MCMULLEN, T. 1998. A lattice model for computing the transmissivity of the cornea and sclera. *Biophysical Journal 75*, 5 (November), 2520–2531.

ANDERSON, R., AND PARRISH, J. 1981. The optics of human skin. *Journal of Investigative Dermatology 77*, 1, 13–19.

ANGELOPOULOU, E. 2001. Understanding the color of human skin. In *Human Vision and Electronic Imaging VI*, SPIE, vol. 4299, 243–251.

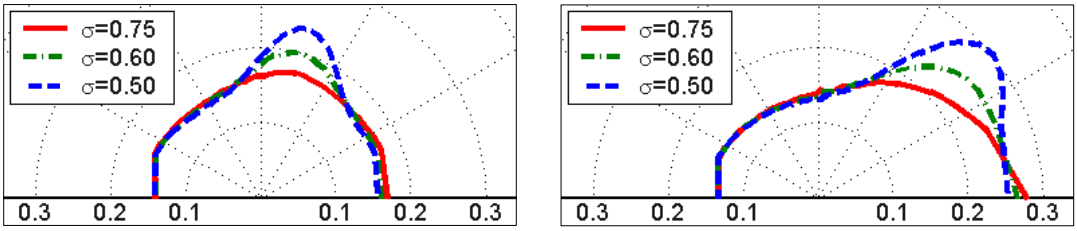

Figure 7: *Comparison of modeled spectral curves provided by the BioSpec model considering variations on the aspect ratio (σ) of the stratum corneum folds. Left: $\theta_i = 15°$. Right: $\theta_i = 45°$.*

Figure 8: *Images generated using the BioSpec model to spectrally simulate erythema conditions. Left: $\vartheta_p = 1.2\%$ and $\vartheta_r = 0.91\%$. Center: $\vartheta_p = 2.7\%$ and $\vartheta_r = 0.3\%$. Right: $\vartheta_p = 3.6\%$ and $\vartheta_r = 0.4\%$.*

BARANOSKI, G., AND ROKNE, J. 1997. An algorithmic reflectance and transmittance model for plant tissue. *Computer Graphics Forum (EUROGRAPHICS Proceedings) 16*, 3 (September), 141–150.

BARANOSKI, G., KRISHNASWAMY, A., AND KIMMEL, B. 2003. Revisiting the foundations of subsurface scattering. Tech. Rep. CS-2003-45, School of Computer Science, University of Waterloo, December.

BRULS, W., AND VAN DER LEUN, J. 1984. Forward scattering properties of human epidermal layers. *Photochem. Photobiol. 40*, 231–242.

CHANDRASEKHAR, S. 1960. *Radiative Transfer*. Dover Publications Inc., New York.

CHURMAKOV, D., MEGLINSKY, I., PILETSKY, S., AND GREENHALGH, D. 2003. Analysis of skin tissues spatial fluorescence distribution by the Monte Carlo simulation. *Journal of Physics D: Applied Physics 36* (July), 1722–1728.

COTTON, S., AND CLARIDGE, E. 1996. Developing a predictive model of skin colouring. In *SPIE Vol. 2708, Medical Imaging 1996*, 814–825.

COTTON, S. 1997. A noninvasive skin imaging system. Tech. Rep. CSR-97-03, School of Computer Science, The University of Birmingham.

DEVLIN, K., CHALMERS, A., WILKIE, A., AND PURGATHOFER, W. 2002. Tone reproduction and physically based spectral rendering. In *Eurographics - State of the Art Reports*, 101–123.

DIFFEY, B. 1983. A mathematical model for ultraviolet optics in skin. *Physics in Medicine and Biology 28*, 647–657.

DOI, M., AND TOMINAGA, S. 2003. Spectral estimation of human skin color using the Kubelka-Munk theory. In *SPIE/IS&T Electronic Imaging*, SPIE, vol. 5008, 221–228.

EVERETT, M., YEARGERS, E., SAYRE, R., AND OLSEN, R. 1966. Penetration of epidermis by ultraviolet rays. *Photochemistry and Photobiology 5*, 533–542.

FARELL, T., PATTERSON, M., AND WILSON, B. 1992. A diffusion theory model of spatially resolved, steady-state diffuse reflectance for the noninvasive determination of tissue optical properties in vivo. *Medical Physics 19*, 879–888.

FLEWELLING, R. 1981. Noninvasive optical monitoring. In *The Biomedical Engineering Handbook*, IEEE Press, Boca Raton, FL, USA, J. Bronzino, Ed., 1–11. Section 86.

FLOCK, S. T., PATTERSON, M. S., WILSON, B. C., AND WYMAN, D. R. 1989. Monte Carlo modeling of light propagation in highly scattering tissues - I: Model predictions and comparison with diffusion theory. *IEEE Transactions on Biomedical Engineering 36*, 12 (December), 1162–1168.

Figure 9: *I*mages generated using the BioSpec model to spectrally simulate jaundice symptoms. Left: $c_{bil} = 0.05g/L$. Center: $c_{bil} = 0.5g/L$. Right: $c_{bil} = 3.0g/L$.

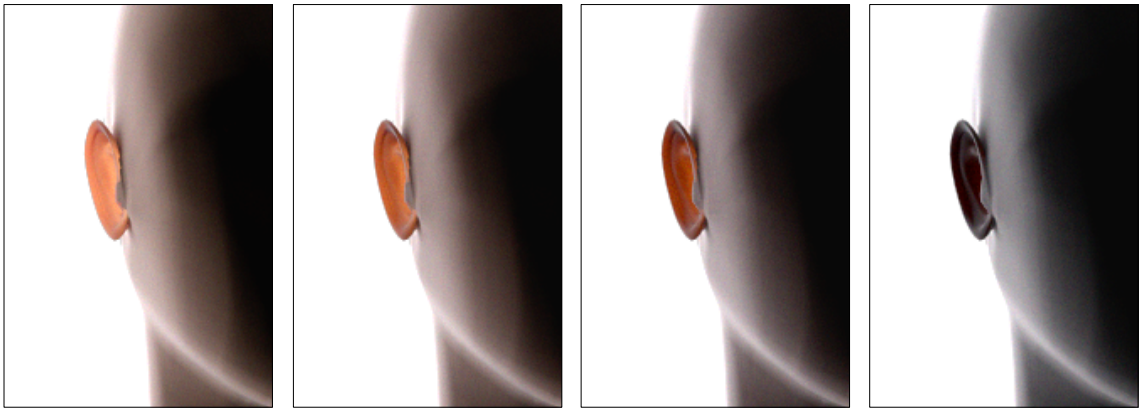

Figure 10: *Images generated using the BioSpec model to show variations in the translucency of skin tissues associated with different levels of melanin pigmentation. From left to right:* $\vartheta_m = 1.9\%$, $\vartheta_m = 5.2\%$ $\vartheta_m = 12\%$ *and* $\vartheta_m = 42\%$.

GLASSNER, A. 1995. *Principles of Digital Image Synthesis*. Morgan Kaufmann Publishers, Inc, San Francisco.

GREENBERG, D., ARVO, J., LAFORTUNE, E., TORRANCE, K., FERWERDA, J., WALTER, B., TRUMBORE, B., SHIRLEY, P., PATTANAIK, S., AND FOO, S. 1997. A framework for realistic image synthesis. In *SIGGRAPH, Annual Conference Series*, 477–494.

HANRAHAN, P., AND KRUEGER, W. 1993. Reflection from layered surfaces due to subsurface scattering. In *SIGGRAPH, Annual Conference Series*, 165–174.

HARO, A., GUENTER, B., AND ESSA, I. 2001. Real-time, photo-realistic, physically based rendering of fine scale human skin structure. In *Rendering Techniques'2001 (Proceedings of the 12th Eurographics Rendering Workshop)*, Springer-Verlag, London, P. M. Hanrahan and W. Purgathofer, Eds., 53–62.

ISHIMARU, A. 1997. *Wave Propagation and Scattering in Random Media*, 2nd ed., vol. 1. IEEE Press, New York.

ISHIMARU, A. 1997. *Wave Propagation and Scattering in Random Media*, 2nd ed., vol. 2. IEEE Press, New York.

JACQUES, S., ALTER, C., AND PRAHL, S. 1987. Angular dependence of HeNe laser light scattering by human dermis. *Lasers in Life Sciences 1*, 4, 309–333.

JACQUES, S. 1996. Origins of tissue optical properties in the uva visible and nir regions. *OSA TOPS on Advances in Optical Imaging and Photon Migration 2*, 364–369.

JENSEN, H., MARSCHNER, S., LEVOY, M., AND HANRAHAN, P. 2001. A practical model for subsurface light transport. In *SIGGRAPH, Annual Conference Series*, 511–518.

LEE, R., MATHEWS-ROTH, M., PATHAK, M., AND PARRISH, J. 1975. The detection of carotenoid pigments in human skin. *Journal of Investigative Dermatology 64*, 175–177.

LENOBLE, J. 1993. *Atmospheric Radiative Transfer*. A. Deepak Publishing, Hampton, Virginia, USA.

LI, S. 2003. Biologic biomaterials: Tissue-derived biomaterials (collagen). In *Biomaterials Principles and Applications*, CRC Press, Boca Raton, USA, J. Park and J. Bronzano, Eds., 117–139.

LIOU, K.-N. 2002. *Introduction to Atmospheric Radiation (2nd. Edition)*. Elsevier Science, San Diego.

MARSCHNER, S., WESTIN, S. H., LAFORTUNE, E., TORRANCE, K., AND GREENBERG, D. 1999. Image-based brdf measurement including human skin. In *Rendering Techniques'1999 (Proceedings of the 10th Eurographics Rendering Workshop)*, Springer-Verlag, Granada, D. Lischinski and G. W. Larson, Eds., 119–130.

MARSCHNER, S., JENSEN, H., CAMMARANO, M., WORLEY, S., AND HANRAHAN, P. 2003. Light scattering from human hair fibers. *ACM Transactions on Graphics 22*, 3, 780–791.

MCCARTNEY, E. 1976. *Optics of the Atmosphere: Scattering by Molecules and Particles*. John Wiley & Sons Inc.

MEGLINSKY, I., AND MATCHER, S. 2001. Modelling the sampling volume for skin blood oxygenation. *Medical & Biological Engineering & Computing 39*, 44–49.

MEGLINSKY, I., AND MATCHER, S. 2003. Computer simulation of the skin reflectance spectra. *Computer Methods and Programs in Biomedicine 70*, 179–186.

NAKAI, H., MANABE, Y., AND INOKUCHI, S. 1998. Simulation analysis of spectral distributions of human skin. In *14th International Conference on Pattern Recognition*, 1065–1067.

NG, C., AND LI, L. 2001. A multi-layered reflection model of natural human skin. In *Computer Graphics International 2001*, 249–256.

NISCHIK, M., AND FORSTER, C. 1997. Analysis of skin erythema using true-color images. *IEEE Transactions on Medical Imaging 16*, 6 (December), 711–716.

NISHITA, T., SIRAI, T., TADAMURA, K., AND NAKAMAE, E. 1993. Display of the earth taking into account atmospheric scattering. *SIGGRAPH, Annual Conference Series*.

PARSAD, D., WAKAMATSU, K., KANWAR, A., KUMAR, B., AND ITO, S. 2003. Eumelanin and phaeomelanin contents of depigmented and repigmented skin in vitiligo patients. *British Journal of Dermatology 149*, 624–626.

POIRIER, G. 2004. Human skin modelling and rendering. Tech. Rep. CS-2004-05, University of Waterloo, January.

PRAHL, S., KEIJZER, M., JACQUES, S., AND WELCH, A. 1989. A Monte Carlo model of light propagation in tissue. *SPIE Institute Series IS 5*, 102–111.

PRAHL, S. 1988. *Light Transport in Tissue*. PhD thesis, The University of Texas at Austin, TX, USA.

PREMOZE, S. 2002. Analytic light transport approximations for volumetric materials. In *Proceedings of the 10th Pacific Conference on Computer Graphics and Applications - Pacific Graphics'2002*, 48–57.

PURGATHOFER, W. 2003. Open issues in photo-realistic rendering. In *Computer Graphics Forum (EUROGRAPHICS Proceedings)*, xix. Invited talk.

RODRIGUEZ, J., YAROSLAVSKY, I., YAROSLAVSKY, A., BATTARBEE, H., AND TUCHIN, V. 2002. Time-resolved imaging in diffusive media. In *Handbook of Optical Biomedical Diagnostics*, SPIE Press, Bellingham, WA, USA, V. Tuchin, Ed., 357–404.

ROLINSKY, B., KÜSTER, H., UGELE, B., GRUBER, R., AND HORN, K. 2001. Total bilirubin measurement by photometry on a blood gas analyser: potential for use in neonatal testing at point of care. *Clinical Chemistry 47*, 10, 1845–1847.

SAIDI, I. 1994. *Transcutaneous optical measurement of hyperbilirubinemia in neonates*. PhD thesis, Rice University, Houston, TX, USA.

SALISBURY, F., AND ROSS, C. 1985. *Plant Physiology*, third ed. Wadsworth Publishing Company, Belmont, California.

SHIMADA, M., YAMADA, Y., ITOH, M., AND YATAGAI, T. 2001. Melanin and blood concentration in human skin studied by multiple regression analysis: assessment by Monte Carlo simulation. *Physics in Medicine and Biology 46*, 2397–2406.

SIMPSON, C., KOHL, M., ESSENPREIS, M., AND COPE, M. 1998. Near infrared optical properties of ex-vivo human skin and subcutaneous tissues measured using the Monte Carlo inversion technique. *Physics in Medicine and Biology 43*, 2465–2478.

STAM, J. 2001. An illumination model for a skin layer bounded by rough surfaces. In *Rendering Techniques'2001 (Proceedings of the 12th Eurographics Rendering Workshop)*, Springer-Verlag, London, P. M. Hanrahan and W. Purgathofer, Eds., 39–52.

STAMNES, K., AND CONKLIN, P. 1984. A new multi-layer discrete ordinate approach to radiative transfer in vertically inhomogeneous atmospheres. *Journal of Quantum Spectroscopy and Radiative Transfer 31*, 3, 273–282.

STRUTT, J. 1871. On the scattering of light by small particles. *Philosophical Magazine 41*, 275 (June), 447–454.

STRUTT, J. 1899. On the transmission of light through an atmosphere containing many small particles in suspension, and on the origin of the blue of the sky. *Philosophical Magazine 47*, 375–384.

SU, Y., WANG, W., XU, K., AND JIANG, C. 2002. The optical properties of skin. In *Optics in Health Care and Biomedical Optics: Diagnostics and Treatment*, SPIE, vol. 4916, 299–304.

TALREJA, P., KASTING, G., KLEENE, N., PICKENS, W., AND WANG, T. 2001. Visualization of the lipid barrier and measurement of lipid pathlength in human stratum corneum. *AAPS PharmSCi 3*, 2, 1–9.

THALMANN, N., KALRA, P., LÉVÊQUE, J., BAZIN, R., BATISSE, D., AND QUERLEUX, B. 2002. A computational skin model: fold and wrinkle formation. *IEEE Transactions on Information Technology in Biomedicine 6*, 4, 317–323.

THODY, A., HIGGINS, E., WAKAMATSU, K., ITO, S., BURCHILL, S., AND MARKS, J. 1991. Pheomelanin as well as eumelanin is present in human dermis. *Journal of Investigative Dermatology 97*, 340–344.

TROWBRIDGE, T., AND REITZ, K. 1975. Average irregularity representation of a rough surface for ray reflection. *Journal of the Optical Society of America 65*, 5 (May), 531–536.

TSUMURA, N., KAWABUCHI, M., HANEISHI, H., AND MIYABE, Y. 2000. Mapping pigmentation in human skin by multi- visible-spectral imaging by inverse optical scattering technique. In *IS&T/SID Eighth Color Imaging Conference*, 81–84.

TSUMURA, N., OJIMA, N., SATO, K., SHIRAISHI, M., SHIMIZU, H., NABESHIMA, H., AKAZAKI, S., HORI, K., AND MIYAKE, Y. 2003. Image-based skin color and texture analysis/synthesis by extracting hemoglobin and melanin information in the skin. In *SIGGRAPH, Annual Conference Series*.

TUCHIN, V. 2000. *Tissue Optics Light Scattering Methods and Instruments for Medical Diagnosis*. The International Society for Optical Engineering, Bellingham, WA, USA.

VAN DE HULST, H. 1980. *Multiple Light Scattering: Tables, Formulas, and Applications*, vol. 1. Academic Press, New York.

VAN DE HULST, H. 1980. *Multiple Light Scattering: Tables, Formulas, and Applications*, vol. 2. Academic Press, New York.

VAN DE HULST, H. 1981. *Light Scattering by Small Particles*, 2nd ed. Dover Publications Inc., New York.

VAN GEMERT, M., JACQUES, S., STERENBORG, H., AND STAR, W. 1989. Skin optics. *IEEE Transactions on Biomedical Engineering 36*, 12, 1146–1154.

VRHEL, M., GERSHON, R., AND IWAN, L. 1994. Measurement and analysis of object reflectance spectra. *Color Research and Application 19*, 1, 4–9.

WANG, L., JACQUES, S., AND ZHENG, L. 1995. MCML – Monte Carlo modelling of light transport in multi-layered tissues. *Computer methods and programs in biomedicine*.

WILSON, B., AND ADAM, G. 1983. A Monte Carlo model for the absorption and flux distributions of light in tissue. *Medical Physics 10*, 824–830.

YAROSLAVSKY, A., PRIEZZHEV, A., RODRIGUEZ, J., YAROSLAVSKY, I., AND BATTARBEE, H. 2002. Optics of blood. In *Handbook of Optical Biomedical Diagnostics*, SPIE Press, Bellingham, WA, USA, V. Tuchin, Ed., 169–216.

YOON, G., WELCH, A., MOTAMEDI, M., AND VAN GEMERT, M. 1987. Development and application of three-dimensional light distribution model for laser irradiated tissue. *IEEE Journal of Quantum Electronics QE-23*, 1721–1733.

ZONIOS, G., BYKOWSKY, J., AND KOLLIAS, N. 2001. Skin melanin, hemoglobin, and light scattering properties can be quantitatively assessed in vivo using diffuse reflectance spectroscopy. *Journal of Investigative Dermatology 117*, 6, 1452–1457.

Appendix A: Rayleigh Scattering

The fundamentals of light scattering begins by examining the event of light scattering with a single particle. One of the fundamental assumptions that be made in order to consider single scattering is independence [van de Hulst 1981]. This means that the particles in a medium are far enough apart that the interaction of light with one particle is not affected by another nearby particle.

Single Scattering

The combination of the scattering and absorption cross sections gives the attenuation cross section represented by:

$$R_{att}(\lambda) = R_{abs}(\lambda) + R_{sca}(\lambda) \tag{15}$$

where:

R_{att} = attenuation cross section,
R_{abs} = absorption cross section,
R_{sca} = scattering cross section.

The general Rayleigh scattering cross section is given by:

$$R_{sca}(\lambda) = \frac{8}{3}\pi k^4 \left|\alpha^2\right| \tag{16}$$

where:
R_{sca} = scattering cross section,
k = wave number (propagation constant in vacuum) $k = \frac{2\pi}{\lambda}$,
α = polarizability.
Note that Equation 16 makes no assumptions about the shape of the particles (represented in the α (polarizability) term).

The absorption cross section for general Rayleigh scattering is given by:

$$R_{abs}(\lambda) = 4\pi k \varrho(i\alpha) \tag{17}$$

where:
$\varrho(i\alpha)$ = complex portion of index of refraction of particle describing permeability.
Again, note that Equation 17 makes no assumption about the shape of the particles either.

The polarizability mentioned in Equation 16 refers to particle polarizability which is affected by the shape and orientation of the particle, and it should not be confused with the polarization of the wave. It is worth noting that the Rayleigh scattering cross section is only valid for particles with relatively small radius ($< 0.05r$) [Ishimaru 1997a; Ishimaru 1997b].

Lord Rayleigh (J.W. Strutt, third Baron of Rayleigh) originally proposed his equations considering dielectric particles [Strutt 1871; Strutt 1899] which exhibit both scattering and absorption. However, models in atmospheric optics omit the absorption cross section due to its negligible impact and its complexity [Lenoble 1993; McCartney 1976; Nishita et al. 1993]. We also choose to omit the absorption cross section with collagen fibers, since the absorption due to collagen fibers is negligible [Ameen et al. 1998].

Phase Function

The phase function mathematically approximates the deflection trajectories of rays when they interact with a particle [van de Hulst 1981; van de Hulst 1980a; van de Hulst 1980b]. A phase function is a probability density function that when given the relative outgoing angle of a deflected particles describes the probability of the particle being deflected in that direction. As with any probability density function, the phase function, in order to be energy conserving must be normalized to unity and satisfy the following equation:

$$\int_{\Omega} \frac{1}{4\pi} p(\cos\theta) d\Omega = 1 \tag{18}$$

where:
$p(\cos\theta)$ = probability of light being scattered in the direction given by the outgoing angle θ.

The Rayleigh phase function for unpolarized light is given by [Chandrasekhar 1960]:

$$p(\cos\theta) = \frac{3}{4}\left(1 + \cos^2(\theta)\right) \tag{19}$$

Scattered Intensity

The intensity of the light scattered in one direction due to Rayleigh scattering is shown in the following equation [van de Hulst 1981]:

$$I = I_o \frac{(1 + cos^2\Theta)k^4 \left|\alpha^2\right|}{2d^2} \tag{20}$$

where:
I = intensity of scattered light,
I_o = intensity of incident light,
Θ = scattering angle,
d = distance to the center of the particle.

For particles that are spherical, we can describe the isotropic polarizability (α) as [van de Hulst 1981]:

$$\alpha = \frac{m^2 - 1}{m^2 + 2} r^3 \tag{21}$$

where:
m = complex refractive index of the particle (=∞ for totally reflecting spheres),
r = radius of the particle.

By substituting $\frac{2\pi}{\lambda}$ for k and Equation 21 into Equation 20, we get the following equation describing the Rayleigh scattering function for spherical particles and incident unpolarized light:

$$I = I_o \frac{8\pi^4(1 + \cos^2\Theta)}{r^2\lambda^4} \left| \left(\frac{m^2 - 1}{m^2 + 2} a^3\right)^2 \right| \tag{22}$$

We can see that this intensity has the characteristic λ^4 dependency. This representation of scattered intensity is useful when trying to evaluate the amount of the incident light that is scattered in a particular direction. Due to the algorithmic nature of the BioSpec model, this expression is not needed in its implementation.

Volume Scattering

The single scattering event describes the process of scattering when light interacts with a single particle. In the case of a medium such as collagen, the size of the particles is very small and thus modelling and simulating the interaction of light with every particle in the medium becomes infeasible. In order to make the problem more tractable, some simplifications and assumptions are essential so that the entire volume containing the particles can be considered.

If we assume that the individual particles within a volume are far enough away from each other so that scattering due to one particle does not affect the the scattering due to another, and that the distribution of these particles is random and homogeneous within the volume, then the effects of single particle scattering can be aggregated over the volume [Ishimaru 1997a; Ishimaru 1997b]. One way of performing this aggregation is to compute the attenuation ratio per unit length and apply Bouger's law. Given this attenuation ratio and the amount travelled in the medium, one can compute the scattering probability of a given ray. However, in order to compute the attenuation ratio, one must know the amount of particles within the volume. This technique, called optical path, or optical depth, has been applied in several atmospheric scattering models [Lenoble 1993], and it has been adapted for collagen fibers [Jacques 1996].

Researchers in atmospheric optics assume the molecules are opaque. One can apply the same assumption for collagen fibers. By using the same formulation used in atmospheric atmospheric optics to derive the scattering coefficient for a volume of air [Lenoble 1993], one can obtain the scattering coefficient for a volume of collagen fibers. In other words, if we take Equation 16 and substitute $\frac{2\pi}{\lambda}$ for k, and if we also assume that the effects of scattering aggregate over all the particles in a volume, we get:

$$R_{sca}(\lambda) = \frac{128\pi^5}{3\lambda^4 N} |\alpha|^2 \tag{23}$$

where:
N = number of particles in the volume (because of aggregate effect).
Now, we can apply the Lorentz-Lorenz formula to derive a value of α for isotropic spheres whose mutual distances are small compared to λ [van de Hulst 1981]. The Lorentz-Lorenz formula is given by:

$$\alpha = \frac{3}{4\pi N} \frac{m^2 - 1}{m^2 + 2} \tag{24}$$

where:
N = number of molecules per unit volume.
However, the complex portion of the index of refraction still poses a problem. In atmospheric radiative transfer the polarizability can be approximated by [Liou 2002]:

$$\alpha = \frac{1}{4\pi N}(\eta^2 - 1) \tag{25}$$

where:
η = real refractive index of the particle.

By using the approximated polarizability factor the scattering (and thus attenuation) cross section becomes:

$$R_{sca}(\lambda) = \frac{8\pi^3 N(\eta^2 - 1)^2}{3\lambda^4 N^2} f(\delta) \tag{26}$$

where:
$f(\delta)$ = anisotropy factor function.

It is worth noting that one still needs to account for the varying index of refraction within the volume. For this purpose, the anisotropy factor function is introduced in atmospheric optics:

$$f(\delta) = \frac{(6 + 3\delta)}{(6 - 7\delta)} \tag{27}$$

where:
δ = anisotropic factor of 0.035 to account for varying index of refraction.
However, we have no evidence to suggest that this anisotropic factor is necessary or relevant for collagen fibres. Hence, for the sake of simplicity, it is not used in our formulation, which results in:

$$R_{sca}(\lambda) = \frac{8\pi^3 N(\eta^2 - 1)^2}{3\lambda^4 N^2} \tag{28}$$

Using this cross section, we can determine the total scattering coefficient by a unit volume of collagen fibers. Researchers in atmospheric optics assume the index of refraction of the medium is vacuum, which is why in Equation 28 the real index of refraction is presented by η alone (expanded, it would be $\frac{\eta}{1.0}$, where 1.0 is the index of refraction of vacuum). In the dermis, however, the collagen fibers are suspended in a medium with its own index of refraction. Therefore, we must represent the index of refraction of this medium. In addition, note that the N term in the numerator can be cancelled. Performing these two operations we get:

$$R_{sca}(\lambda) = \frac{8\pi^3 (\left(\frac{\eta_f}{\eta_m}\right)^2 - 1)^2}{3\lambda^4 N} \tag{29}$$

Multiplying $R_{sca}(\lambda)$ by the distance travelled in the medium gives the quantity described in Equation 5. Since we are dealing with small collagen fibers rather than molecules of oxygen, we must determine the number of particles in the volume. According to Jacques [Jacques 1996], we can simulate Rayleigh scattering within the dermal layers using spheres (of radius r). Considering that 21% of the dermis is composed of collagen fibers [Jacques 1996], we can can compute the number of particles in the volume as:

$$N = \frac{0.21}{V_s} \tag{30}$$

where:
V_s = volume of the sphere $\left(\frac{4}{3}\pi r^3\right)$.

If light is successfully scattered in a volume of collagen fibers, we need to compute the direction in which the light is scattered. Recall that the Rayleigh phase function can be seen as a probability density function which describes the probability of a wave being scattered in a particular direction. Hence, given random numbers uniformly distributed in the interval $[0..1]$, we can compute a direction of scattering using the perturbation angles given in Equation 4.